Weather and Climate Extremes 54 (2026) 100955

Contents lists available at ScienceDirect

Weather and Climate Extremes

journal homepage: www.elsevier.com/locate/wace

Sub-seasonal variability of extreme heatwaves in eastern China and its structural linkage to the Tibetan Plateau atmospheric heat source

Meirong Wang [a,d,e], Shuaiyi Li [a,c], Zhongshui Yu [d,e], Zhu Zhu [f], Jun Wang [b,*]

[a] State Key Laboratory of Climate System Prediction and Risk Management, Key Laboratory of Meteorological Disaster, Ministry of Education, Collaborative Innovation Center on Forecast and Evaluation of Meteorological Disasters, Nanjing University of Information Science and Technology, Nanjing, China
[b] International Institute for Earth System Science, Nanjing University, Nanjing, China
[c] Department of Atmospheric and Oceanic Sciences and Institute of Atmospheric Sciences, Fudan University, Shanghai, China
[d] Xizang Mêdog Field Scientific Observation and Research Station for Atmospheric Water Cycle, Mêdog, China
[e] Xigazê National Climate Observatory, CMA, Xigazê, China
[f] College of Meteorology and Oceanography, National University of Defense Technology, Changsha, China

ARTICLE INFO

Keywords:
Extreme heatwaves
Tibetan Plateau
Atmospheric heat source
Sub-seasonal variability
East Asian summer circulation

ABSTRACT

Recent extreme heatwaves in eastern China have caused escalating socio-economic and environmental vulnerabilities. This study identifies distinct sub-seasonal variability in summer heatwaves, with the North China Plain (NCP) prominently affected in June and the Yangtze River Valley (YRV) during July–August (JA). The Tibetan Plateau atmospheric heat source (TP AHS) exhibits corresponding spatial differences, displaying significant interannual co-variability with regional heatwave features. During June, an intensified TP AHS is accompanied by a southward displacement of the upper-level westerly jet stream, driving differential thermal advection and deep subsidence over the NCP. Spatially overlapping with this aloft downwelling, the westward expansion of the western Pacific subtropical high (WPSH) aligns with a positive horizontal temperature advection center over the NCP, closely tied to an anomalous mid-to-lower tropospheric cyclonic circulation along the northern flank of the WPSH. During JA, the enhanced TP AHS corresponds to a northward jet stream shift and a northwestward relocation of the South Asian High (SAH), establishing anomalous upper-level convergence over the YRV. These multi-scale circulation configurations, together with a V-shaped isentropic downglide structure radiating from the TP, form a coherent dynamic framework driving persistent subsidence over the YRV. Additionally, these dynamically aligned subsidence zones feature prominent cloud reduction that enhances surface downward solar radiation and sensible heat flux. Through a land–atmosphere coupling loop, these localized diabatic feedbacks structurally match the enhanced intensity and persistence of regional extreme heatwaves. These findings demonstrate that the TP AHS exhibits a month-dependent configuration structurally coupled with sub-seasonal heatwaves across eastern China, co-varying with 35–51% of the extreme heatwave days. This provides process-level insights into the physical linkages between upstream TP thermal anomalies and downstream thermodynamic extremes.

1. Introduction

In recent years, alongside the intensification of global warming, the frequency and intensity of extreme heatwaves have significantly increased worldwide, exerting profound impacts on human society, ecosystems, and economic development (Robine et al., 2008; IPCC, 2021; Alizadeh et al., 2022; Wang et al., 2023). Eastern China, as a densely populated and economically developed region, faces prominent threats from extreme heatwaves (Sun et al., 2018, 2022; Piao et al., 2010; Zhao, 2020; Zhang et al., 2024; Zhou et al., 2025). In 2013, a severe heatwave affected most regions of eastern China, causing the average summer temperature to rise by 0.82°C and resulting in an estimated direct economic loss of 8 billion USD. By 2022, the situation had intensified, with a prolonged heatwave lasting approximately 79 days in east-central China, leading to recorded unprecedented daily maximum temperatures in most regions (Hao et al., 2023; Jiang et al., 2023; Liang et al., 2024; Ni et al., 2024; Tan et al., 2024; Ma et al., 2025). Therefore, understanding the variability, associated

* Corresponding author.
E-mail address: wangjun@nju.edu.cn (J. Wang).

https://doi.org/10.1016/j.wace.2026.100955
Received 11 July 2025; Received in revised form 3 September 2026; Accepted 3 September 2026
Available online 7 September 2026

mechanisms, and predictable sources of extreme heatwaves in eastern China is critically important.

Previous studies have indicated that formation and evolution of extreme heatwaves in eastern China are closely associated with multiple factors, including global warming (Sun et al., 2014; Ma et al., 2017; Zhang et al., 2024), atmospheric circulation anomalies (Wang et al., 2016; Li et al., 2021; Qian et al., 2024; Shi et al., 2025), sea surface temperature variations (Arblaster and Alexander, 2012; Chen and Zhou, 2018; Jiang et al., 2025), urbanization processes (Yang et al., 2015; Lin et al., 2024; Zheng et al., 2024; Peng et al., 2024), and human activities (Freychet et al., 2017; Kong et al., 2024; He and Chen, 2024; Liang et al., 2024). The western Pacific subtropical high (WPSH) is widely recognized as the primary atmospheric circulation system that exerts dominant control over the summer heatwaves across eastern China, particularly through its variations in intensity and westward expansion (Li et al., 2015, 2023; Luo and Lau, 2018; Choi and Kim, 2019; Deng et al., 2020; J. L. Jiang et al., 2024). Liu et al. (2019) found that a stronger and more westward-extending WPSH tends to increase heatwaves in eastern China. Additionally, in terms of the regional distribution, the Yangtze River Valley (YRV) and south China experience particularly intense heatwaves (Luo and Lau, 2018; Cao et al., 2022; Peng et al., 2024; Hu et al., 2024), while northeast and north China have also faced growing heatwave impacts in recent years (Kang and Eltahir, 2018; Tao and Zhang, 2019; Xiao et al., 2024). In June 2023, a record-breaking extreme heatwave occurred in North China Plain (NCP), with daily peak temperatures climbing above 40°C in a widespread area (Qian et al., 2023). Notably, Deng et al. (2019) found that the primary influencing systems of extreme heatwaves differ substantially across different regions of eastern China (NCP, YRV, and South China), suggesting that a uniform spatial framework is insufficient for clarifying downstream meteorological responses.

Tibetan Plateau (TP), as a sensitive area to global warming, plays an important role in modulating the climate changes of East Asia and even the globe (Duan et al., 2006; Wu et al., 2007; Yao et al., 2019). The thermal conditions of the TP exert a profound influence on extreme weather events in East Asia (Wu et al., 2012, 2015; Ge et al., 2019; Dong et al., 2019; Diallo et al., 2022). Numerous studies have discussed the linkage between TP thermal conditions and Eurasian heatwaves (Wu et al., 2016; Shi et al., 2024; Dong et al., 2024a). Although studies on the relationship between TP's thermal effects and extreme heatwaves over eastern China are still relatively limited, they have increasingly attracted research attention in recent years (Wu et al., 2012; Deng et al., 2023; W. Jiang et al., 2024; Dong et al., 2024b). Lu et al. (2024) contrasted the responses of heatwave to TP thermal anomalies during the 2013 and 2022 summers, highlighting the crucial effect of TP thermal variability. This relationship maintains its validity across various time scales, from decadal fluctuations (Wu et al., 2012) to long-term trends (Tan et al., 2023, 2025), throughout eastern and northwest China. In fact, heatwaves exhibit obvious subseasonal-to-seasonal (S2S) variations, governed by different physical processes in different months (Wang et al., 2023). Jiang et al. (2023) analyzed the month-to-month variations of extreme heatwaves during the summer of 2022, and found that monthly mean atmospheric circulation anomalies were insufficient to account for the heatwaves in June; specifically, the July high temperature and drought events were closely associated with distinct local soil moisture, while anomalous atmospheric circulation patterns emerged as the dominant factor modulating the August heatwaves.

Unlike previous studies that primarily focused on case analyses or summer seasonal means of extreme heatwaves, this research utilizes long-term multi-source datasets to systematically examine the S2S variability of extreme heatwaves across eastern China during summer months. We evaluate its concurrent association with the atmospheric heat source (AHS) over the TP, and discuss the underlying physical mechanisms through comprehensive diagnostic analyses.

The remainder of this paper is organized as follows. Section 2 describes the data and methodology employed in our study. In Section 3.1 and 3.2, we examine the S2S characteristics of summer heatwaves over eastern China and their association with TP AHS. Section 3.3 and 3.4 present the associated large-scale circulation patterns and underlying physical mechanisms. Finally, Section 4 provides concluding remarks and discusses the implications of our findings.

2. Data and methods

2.1. Data

The daily maximum surface (2 m) air temperature data, spanning 1979 to 2022, were provided by the National Meteorological Information Center of the China Meteorological Administration (CMA). These station-based data were interpolated into a gridded format, known as CN05.1, featuring a high horizontal resolution of 0.25° × 0.25°(Wu and Gao, 2013). To examine the large-scale atmospheric background and structural features of the heat source, the Japanese 55-year Reanalysis (JRA-55) dataset was employed (Kobayashi et al., 2015). The utilized variables include geopotential height (z), zonal and meridional winds (u, v), vertical velocity (ω), temperature (T), potential temperature (θ), shortwave radiation fluxes, surface sensible heating flux, and total cloud cover fraction. All reanalysis products feature a horizontal resolution of 1.25° × 1.25° on standard pressure levels.

2.2. Methods

The thermal condition over the TP can be effectively characterized by the vertically integrated atmospheric apparent heat source (<Q_1>), which provides a comprehensive measure of diabatic heating processes within the atmospheric column. In this study, it can be calculated via the residual budget equations (Yanai et al., 1973) using the JRA-55 reanalysis dataset. The equations are given as follows:

$$Q_1 = C_p\left[\partial T/_{\partial t} + \boldsymbol{V}\cdot\nabla T + \left(p/_{p_s}\right)^k \omega(\partial\theta/\partial p)\right], \quad (1)$$

$$\langle Q_1\rangle = \frac{1}{g}\int_{200}^{p_s} Q_1 \mathrm{d}p, \quad (2)$$

where Q_1 is atmospheric apparent heat source on a single pressure level, and $\langle Q_1\rangle$ represents its column-integrated counterpart calculated from the surface pressure (p_s) to the 200 hPa level. The variable $\boldsymbol{V}$ denotes the horizontal wind vector, and p is the air pressure. C_p is the specific heat of dry air at constant pressure (1 004 J kg^{-1} K^{-1}), g is the acceleration of gravity, and $k \approx 0.286$.

The reliability of JRA-55-derived <Q_1> over the TP has been extensively validated across multiple timescales (Wang et al., 2019a, 2019b; Zhu et al., 2025). JRA-55 exhibits a robust spatial alignment with observations regarding long-term trends and shows high consistency with ERA-Interim on interannual scales. On S2S scales, discrepancies among multi-source reanalysis datasets narrow significantly, and JRA-55 successfully captures the periodic evolution of the summer TP heat source. Furthermore, it realistically reproduces the regional diurnal convective heating (Chen et al., 2014) and atmospheric thermal structures comparably to ERA5 (Luo et al., 2025), confirming its high dependability for investigating TP AHS variability.

Extreme heatwave events can be defined using either absolute or relative threshold criteria. Relative thresholds, commonly based on percentile approaches, are highly effective for capturing geographical variations in temperature extremes. In contrast, absolute thresholds offer a more intuitive and standardized framework for localized impact assessments. In this study, we adopt the absolute threshold of 35°C, as standardized by the CMA, to identify extreme heatwave events. This absolute criterion aligns closely with the 95th percentile-based relative threshold for summertime extreme high temperatures over key regions of eastern China (Deng et al., 2019). Following the CMA's operational classification (Zhai and Pan, 2003), a specific day is designated as an extreme heatwave event when the daily maximum surface air temperature (T_{max}) reaches or exceeds 35°C.

To investigate the interannual variability of extreme heatwaves across eastern China and their associated mechanisms, all climate variables were first linearly detrended to eliminate the confounding signals of long-term warming trends. A 2–7-year band-pass Lanczos filter was subsequently applied to isolate the interannual signals. This filtering procedure was performed on the full dataset covering 1979–2022, while the subsequent diagnostic analyses were restricted to the reliable window of 1981–2020 to thoroughly eliminate edge effects. Crucially, since band-pass filtering introduces pronounced artificial autocorrelation and systematically reduces the independent sample size, the effective degrees of freedom were rigorously adjusted following Bretherton et al. (1999) before statistical testing. Owing to the reduction in the effective sample size imposed by this conservative correction, a 90% confidence level was systematically adopted for mapping the anomalous circulation and thermodynamic fields. This choice is physically motivated to maintain the geographic continuity and large-scale geometric features; under stricter criteria, certain derivative variables that are highly sensitive to small-scale noise tend to become artificially fragmented. To verify the statistical robustness of our findings, a more stringent 95% confidence threshold was applied. The resulting supplementary fields (Fig. S1–S5) exhibit highly convergent spatial patterns with the primary figures. Crucially, the prominent features in our target regions remain statistically significant at this elevated level, demonstrating that the core conclusions are insensitive to threshold selection.

3. Results

3.1. Sub-seasonal variations in heatwaves across eastern China

Fig. 1 illustrates the spatial distribution of the climatological mean extreme heatwave days across eastern China during the entire summer season (June–August) from 1979 to 2022. The spatial pattern reveals pronounced regional heterogeneity, characterized by two primary hotspots where extreme heatwave events exhibit the highest frequency: the

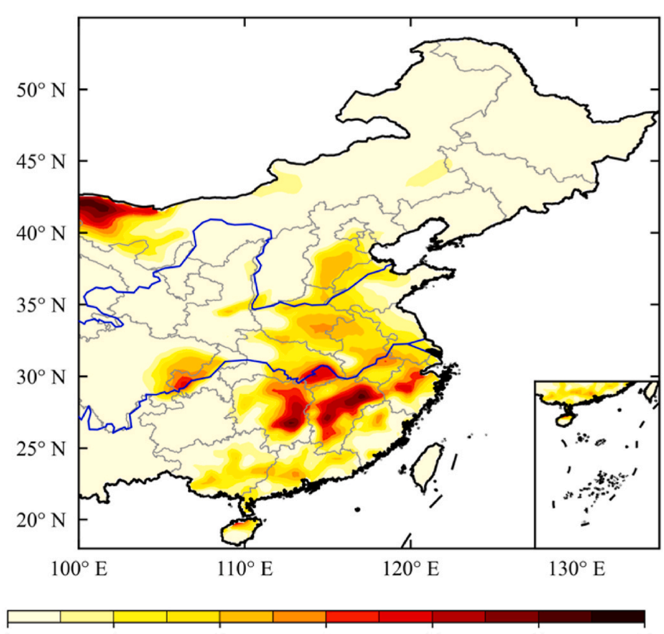

Fig. 1. Spatial distribution of the climatological mean extreme heatwave days (units: days) over eastern China during the summer season (June-July-August) from 1979 to 2022.

NCP and the YRV. In particular, core sectors with provinces such as Jiangxi and Hunan experience more than 30 extreme heatwave days per summer on average, highlighting a substantial regional exposure to persistent high-temperature conditions. Given the region's dense population and high concentration of economic activities, these localized thermal configurations imply considerable socio-economic and public health risks.

Further analysis indicates that this spatial heterogeneity of summer extreme heatwaves across eastern China is closely linked to its sub-seasonal variability, manifesting as substantial year-by-year fluctuations. Specifically, extreme heatwaves in the NCP mainly cluster in June, whereas the YRV experiences more frequent and intense heatwaves during July and August. To better characterize these temporal shifts, regional averages for these key domains were calculated for each month, followed by composite analyses of high-temperature days between strong and weak years (Fig. S6). The composite results further confirm the distinct, month-dependent sub-seasonal regimes of extreme heatwaves across eastern China.

Due to the highly congruent spatial patterns observed in July and August (Fig. S6), these two months (hereafter abbreviated as JA) were combined for subsequent analyses. A comparative composite analysis between strong and weak heatwave years–defined by a ±0.5 standard deviation (σ) threshold to balance statistical sample size and anomaly amplitude–reveals a significant prolongation of extreme heatwave durations. During JA, the positive composite differences of heatwave days are predominantly concentrated across the YRV region, with maximum anomalies exceeding 15 days, particularly in Hunan, Jiangxi, and Zhejiang provinces (Fig. 2c). In contrast, June exhibits a geographically distinct focus, with significant heatwave anomalies exceeding 6 days primarily restricted to the NCP (Fig. 2a and Fig. S6a).

The interannual time series of extreme heatwave frequency further highlight the distinct temporal behaviors between June (Fig. 2b) and JA (Fig. 2d). The variations between these two summer phases show remarkably low consistency with a non-significant correlation, further demonstrating that the early summer (June) and peak summer (JA) heatwave regimes over eastern China are closely tied to decoupled atmospheric configurations. Importantly, sensitivity tests using stricter classification criteria (e.g., employing an anomaly threshold of ±1.0 σ) yield highly consistent results. This coherence demonstrates that the distinct temporal behaviors and decoupled interannual variations between the two summer phases represent a robust physical feature rather than an artifact of threshold selection.

3.2. Relationship with TP atmospheric heat source

The thermal forcing over the TP during summer exhibits a close alignment with downstream weather systems, including the development of extreme heatwaves. To elucidate this linkage, we investigate the sub-seasonal relationship between TP thermal anomalies and extreme heatwaves over eastern China. As a prerequisite, we examine the sub-seasonal features of the interannual variability in the summer TP AHS. Fig. 3 presents the leading empirical orthogonal function (EOF) modes of interannual variability in the TP AHS during June and JA for the period 1981–2020, along with their corresponding principal components (PC1).

In June, the EOF1 pattern, which explains 28.75% of the total variance, is characterized by broad coherent anomalies across most regions, contrasted by localized opposite-phase signals over the western and central TP (Fig. 3a). In contrast, the JA pattern features a distinct multipole structure with alternative anomaly centers arranged in a southeast-to-northwest orientation, accounting for 21.47% of the total variance (Fig. 3c). These results highlight that prominent sub-seasonal shifting also exists within the dominant modes of the TP AHS. Additionally, the associated PC1 time series for June and JA exhibit pronounced interannual fluctuations (Fig. 3b and d) and are significantly correlated with the corresponding heatwave indices shown in Fig. 2b and d ($r = 0.36$ and

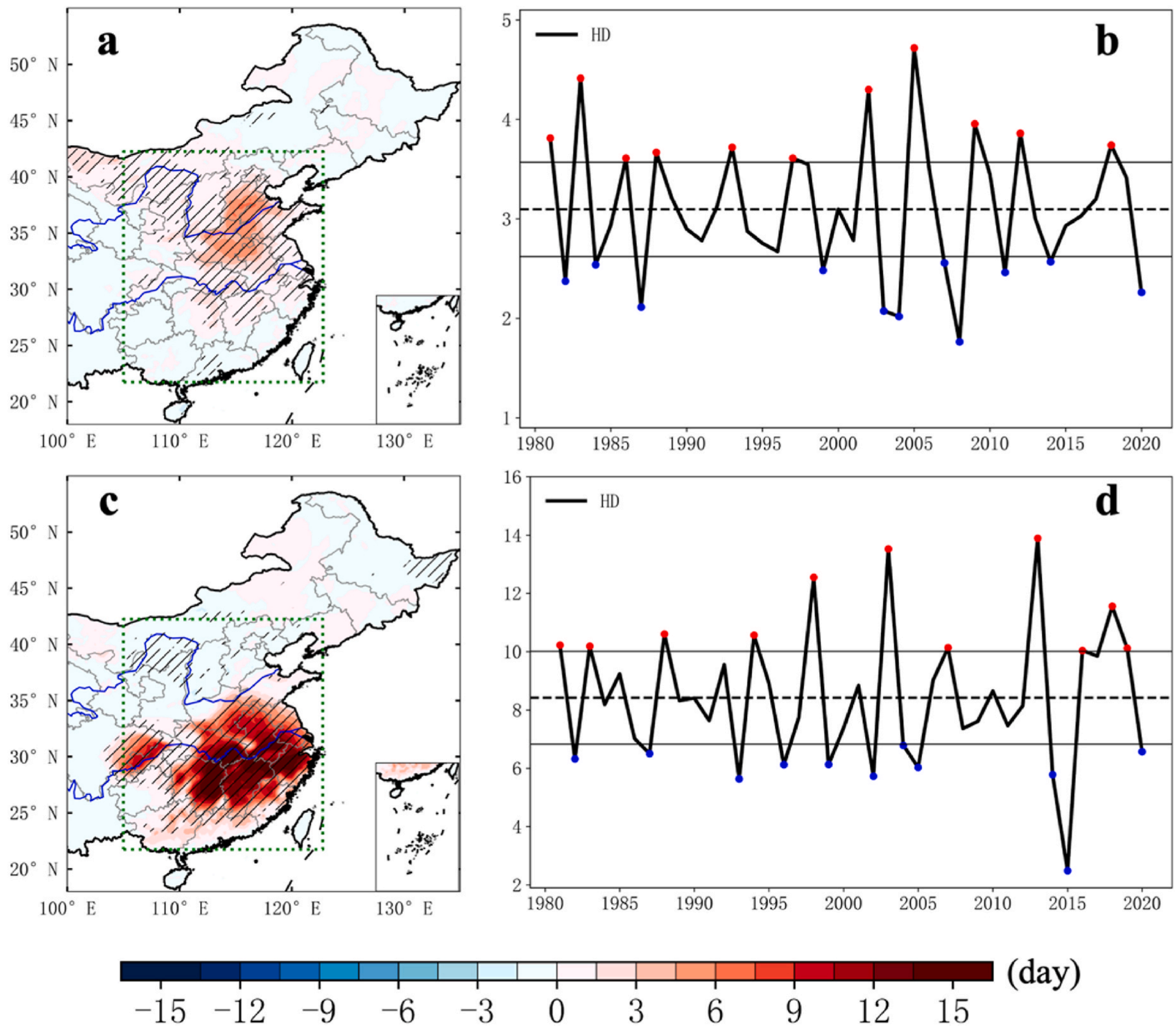

Fig. 2. Spatial distributions of the differences in extreme heatwave days during (a) June and (c) July–August (JA) between strong and weak extreme heatwave years over eastern China during 1981–2020. Hatched areas indicate regions exceeding the 90% confidence level based on a two-tailed Student's t-test. Panels (b) and (d) show the corresponding interannual time series of regionally averaged extreme heatwave days over eastern China (outlined by the green boxes) in June and JA, respectively, with red and blue dots marking the identified strong and weak years.

0.40, respectively; $p < 0.05$). This robust co-variability implies a potential physical teleconnection between TP thermal forcing and downstream heatwave regimes.

To further confirm this linkage, we conducted composite analyses of the TP AHS anomalies between strong and weak extreme heatwave years for June and JA, respectively (Fig. S7). Strikingly, the resulting composite difference patterns closely resemble their counterpart EOF1 modes shown in Fig. 3a and c, thereby reinforcing the remarkable sub-seasonal characteristics of the TP thermal forcing. In June, significantly positive AHS anomalies are dynamically concentrated over the southern and southwestern TP, complemented by pronounced negative anomalies over the east-central sector (Fig. S7a), resembling the primary features of the EOF1 pattern. During JA, a well-defined multi-pole configuration emerges across the TP (Fig. S7b), which is highly congruent with the EOF1 modality and reflects the spatial features of downstream heatwave variability. These composite results further underscore a robust sub-seasonal coupling between the TP thermal anomalies and the occurrence of extreme heatwaves over eastern China.

To systematically investigate the statistical relationship between the TP AHS and downstream extreme heatwaves, we performed a composite analysis based on the PC1 time series of TP AHS. Years with high and low AHS anomalies were identified using a ± 0.5 standard deviation threshold of the PC1 index, allowing for a robust comparison of downstream extreme heatwave activities under contrasting TP thermal conditions. As illustrated in Fig. 4a and b, the spatial anomalies of extreme heatwaves exhibit a striking sub-seasonal shift that closely co-varies with the seasonal evolution of the TP AHS. Specifically, positive TP AHS anomalies in June are predominantly accompanied by increased extreme heatwave frequencies over the NCP (Fig. 4a), whereas the peak-summer (JA) thermal anomalies over the TP correspond to a southward shift of the heatwave footprint toward the YRV region (Fig. 4b). These patterns align well with the independent composite analysis shown in Fig. 2, verifying the robust subseasonal co-variability between the TP AHS and downstream heatwave regimes.

Crucially, we quantified the statistical alignment between the two phenomena by calculating the fractional share of extreme heatwave days that concurrently occur with prominent TP AHS anomalies (Fig. 4c and d). In terms of statistical covariance, TP thermal forcing matches approximately 30%–60% of the extreme heatwave days across key areas of the NCP in June (Fig. 4c) and around 50% over the YRV during JA (Fig. 4d). Notably, the tightest statistical linkage occurs over the upper YRV, spanning eastern Sichuan and Chongqing in JA, where over 80% of extreme high-temperature days directly coincide with periods of enhanced TP thermal anomalies (Fig. 4d). This exceptionally high spatial correspondence aligns well with their immediate downstream location and geographical proximity to the eastern flank of the TP.

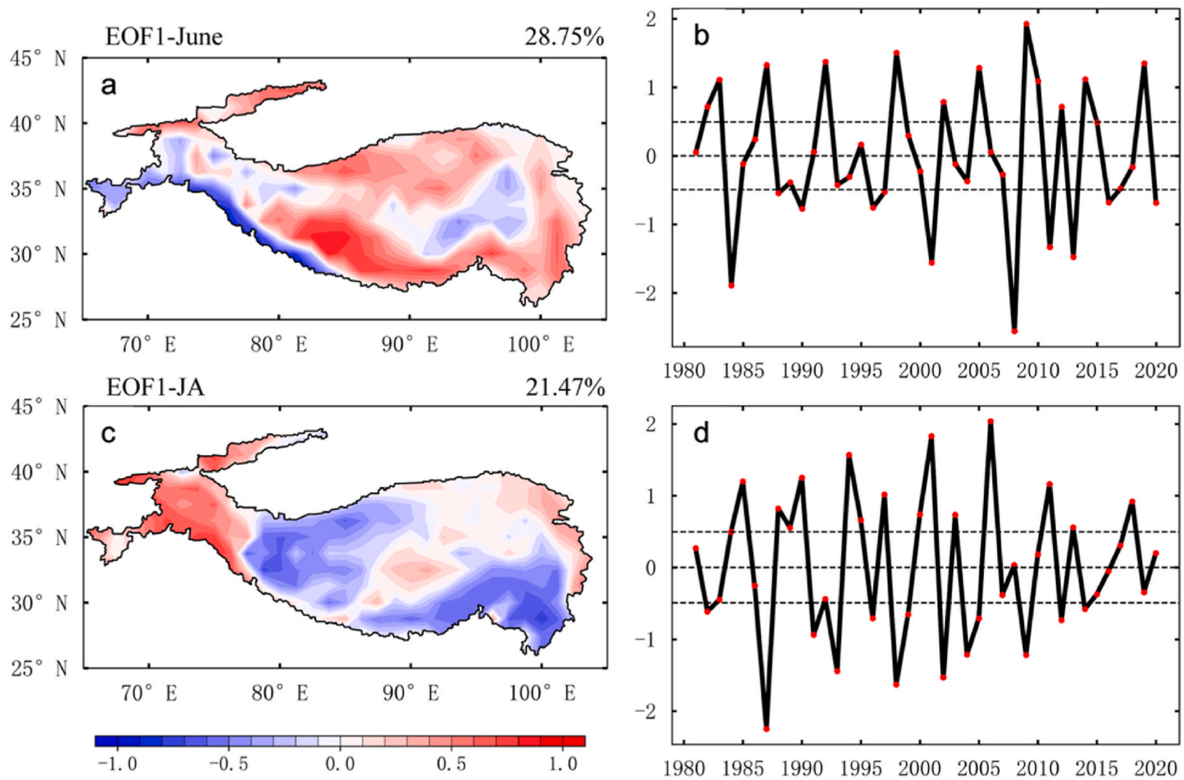

Fig. 3. Spatial patterns of the first leading empirical orthogonal function mode (EOF1) of the vertically integrated apparent heat source (<Q_1>) over the TP in (a) June and (c) JA during 1981–2020, along with their corresponding principal component (PC1) time series shown in (b) and (d), respectively.

Statistical analysis reveals a pronounced sub-seasonal contrast in extreme heatwave coverage across eastern China during 1981–2020. In June, a cumulative total of 3 207 grid points are affected by extreme heatwaves, whereas this number increases markedly to 15762 grid points during JA (Fig. 2a and c). Even considering that the temporal span of JA is twice that of June, this nearly five-fold expansion in cumulative spatial extent reflects a substantial intensification and broader geographical footprint of high-temperature extremes during peak summer. When concurrent with prominent TP AHS anomalies, the overlapping grid points total 1 127 (accounting for 35.1% of the June heatwave extent) over the NCP, and 8064 (accounting for 51.2% of the JA heatwave extent) over the YRV (Fig. 4a and b). Collectively, these statistical results demonstrate: (1) a multi-fold greater spatial coincidence between the TP AHS and eastern China heatwaves during JA relative to June, and (2) distinct regional preferences in their sub-seasonal co-variability, characterized by a dominant spatial alignment over the YRV during peak summer. Together, these findings highlight a pronounced sub-seasonal and regional heterogeneity within the TP AHS-heatwave relationship, providing empirical statistical insights that offer valuable sub-seasonal predictive implications for downstream extreme thermal events.

3.3. Large-scale circulation features and potential dynamic pathways

The sub-seasonal contrast in extreme heatwave distribution across eastern China is accompanied by distinct configurations of large-scale atmospheric circulation associated with TP thermal anomalies. Fig. 5 illustrates the upper-level westerly jet structures during June and JA, categorized by contrasting states of the TP AHS. In June (Fig. 5a and b), the climatological jet stream core is positioned south of 40°N, extending zonally across the northern TP and downstream over the NCP. During years with an enhanced June TP AHS, a pronounced asymmetric configuration emerges, characterized by prominent positive westerly anomalies along the southern flank of the climatological jet axis.

This configuration corresponds to intensified vertical wind shear in the middle-to-upper troposphere over the targeted downstream region (30°N–40°N, Fig. 5b). In accordance with thermal wind balance, this enhanced vertical shear is structurally coupled with a steeper meridional temperature gradient aloft, coinciding with anomalous cold-air advection in the upper troposphere. Within the framework of the quasi-geostrophic omega equation, this differential thermal advection acts as a key dynamic forcing that drives large-scale descending motion over the NCP (Fig. 6a). Crucially, while this forced downwelling originates aloft, its downward propagation induces deep, column-wide adiabatic compression, which efficiently suppresses local cloud formation and amplifies near-surface diabatic warming.

In contrast, during peak summer (JA), the climatological westerly jet stream migrates northward, positioning its core well north of 40°N (Fig. 5c and d). Concurrently, an enhanced TP AHS is accompanied by a further northward shift of the jet stream axis, inducing a distinct easterly anomaly along its southern periphery directly overlying the YRV region (Fig. 5c and d). This configuration is highly coherent with pronounced localized subsidence (Fig. 6b), manifesting as a complex three-dimensional circulation response that is further elaborated through the coupled diagnostic framework of Fig. 7. Moreover, during the June-to-August transition, the YRV is structurally positioned on the right (equatorward) side of the upper-level jet exit region, a quadrant typically characterized by upper-level convergence. This synoptic configuration spatially aligns with suppressed vertical motion, thereby providing a favorable dynamical background for the clustering of localized extreme heatwaves during JA.

Additionally, a coherent sub-seasonal transition in the vertical velocity field is observed over eastern China, featured by anomalous ascending motion over South China in June that shifts northward toward the NCP during JA (Fig. 6). This spatiotemporal evolution is highly synchronized with the sub-seasonal northward migration of the East Asian summer monsoon rain belt, further highlighting the tight dynamic linkage between large-scale circulation transitions and the development

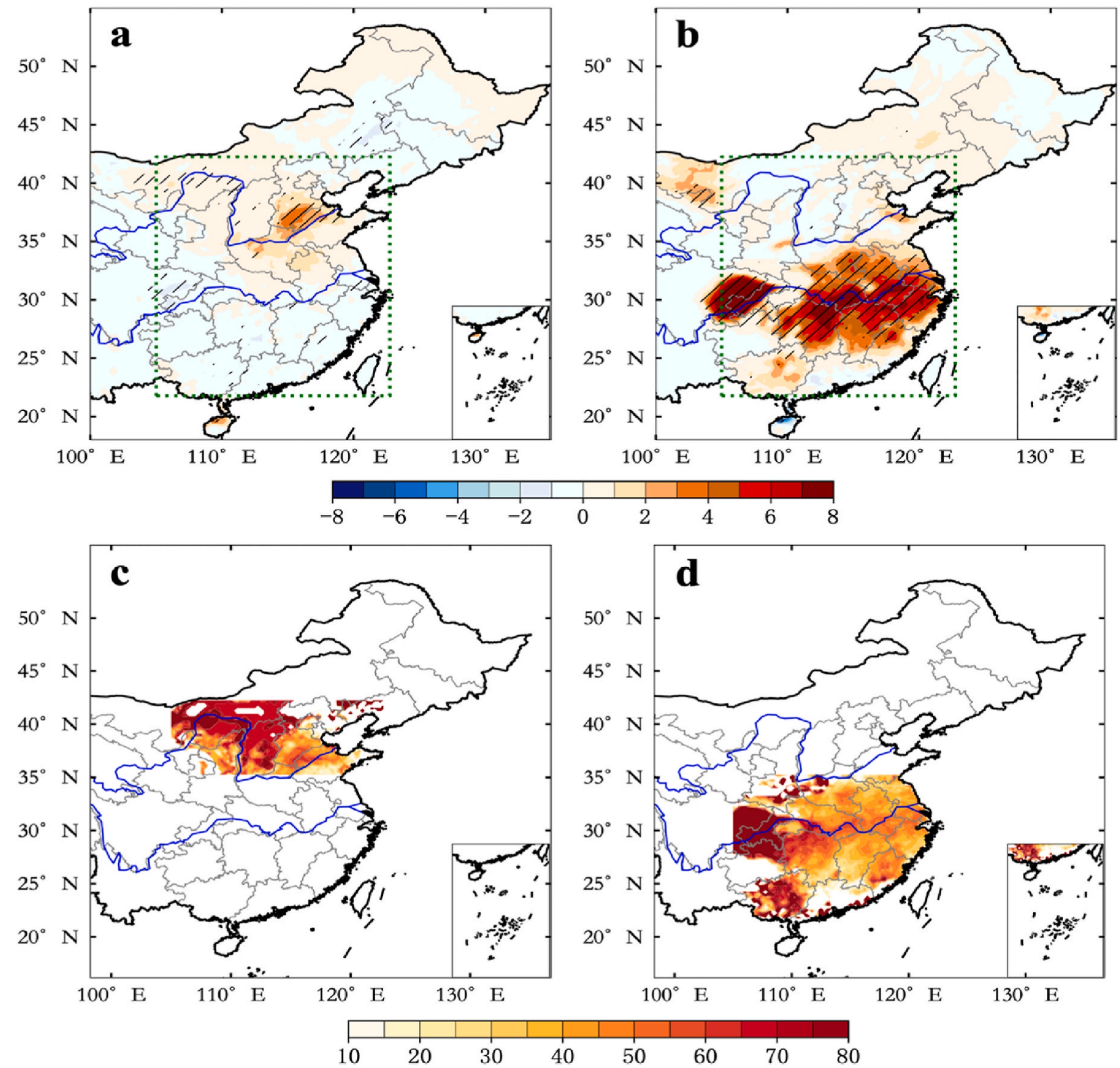

Fig. 4. Spatial patterns of the composite differences in extreme high-temperature days (days) over eastern China between strong and weak TP $<Q_1>$ years during (a) June and (b) JA from 1981 to 2020. Hatched areas indicate regions exceeding the 90% confidence level. Panels (c) and (d) illustrate the statistical proportions of extreme heatwave days concurrently occurring with prominent TP $<Q_1>$ anomalies relative to the total heatwave days in June and JA, respectively.

of regional sub-seasonal thermal extremes.

We further examine the upper- and lower-level coupled circulation fields during JA (Fig. 7) to fully characterize the three-dimensional structures associated with the prominent zonal wind anomalies identified in Fig. 5d. Horizontally, a pronounced barotropic anticyclonic anomaly is clearly evident over the NCP and adjacent coastal waters. Simultaneously, another prominent anticyclonic anomaly is centered to the west of the TP, forming a paired circulation structure flanking the TP. Positioned on either side of the TP, these dual anticyclonic configurations jointly drive a robust easterly flow anomaly along and north of the 30°N (Fig. 7a and c), consistent with Fig. 5d.

Radiating directly from intense convective heating over the TP, two distinct centers of positive potential temperature anomalies reside on the western and eastern flanks of the TP, establishing a characteristic V-shaped isentropic structure (Fig. 7b). Thermodynamically, this V-shaped thermal configuration couples with the flanking anticyclonic pair. In accordance with hydrostatic balance and quasi-geostrophic potential vorticity (QGPV) inversion, these deep tropospheric warm centers aloft modify local thickness fields, acting as negative PV anomalies that dynamically anchor the dual anticyclonic anomalies on both side of the TP. Within this coupled thermodynamic environment, the anomalous easterly flows flank the TP, laying the structural foundation for distinct localized vertical overturning responses between the upstream and downstream regions (Fig. 7d).

To explicitly clarify the underlying dynamics producing this asymmetric vertical velocity response—specifically why descent prevails to the east rather than the west of the TP—we interpret the structural configuration through the framework of thermally forced atmospheric adaptation and the adiabatic omega equation on isentropic surfaces (the upglide/downglide mechanism). In response to intense convective heating over the TP, the atmosphere exhibits a classic Gill-type thermodynamic response that sustains the V-shaped slope of potential temperature surfaces away from the TP flanks, a configuration consistent with the theoretical framework of He et al. (2023). Under this geometric framework, the enhanced horizontal wind anomalies interact distinctively with these tilted isentropic surfaces. On the eastern flank of the TP (over the YRV region), the anomalous easterlies blow dynamically across the downstream thermal gradient, establishing a robust isentropic downglide process where the anomalous flow glides downward along the eastward-sloping potential temperature surfaces towards

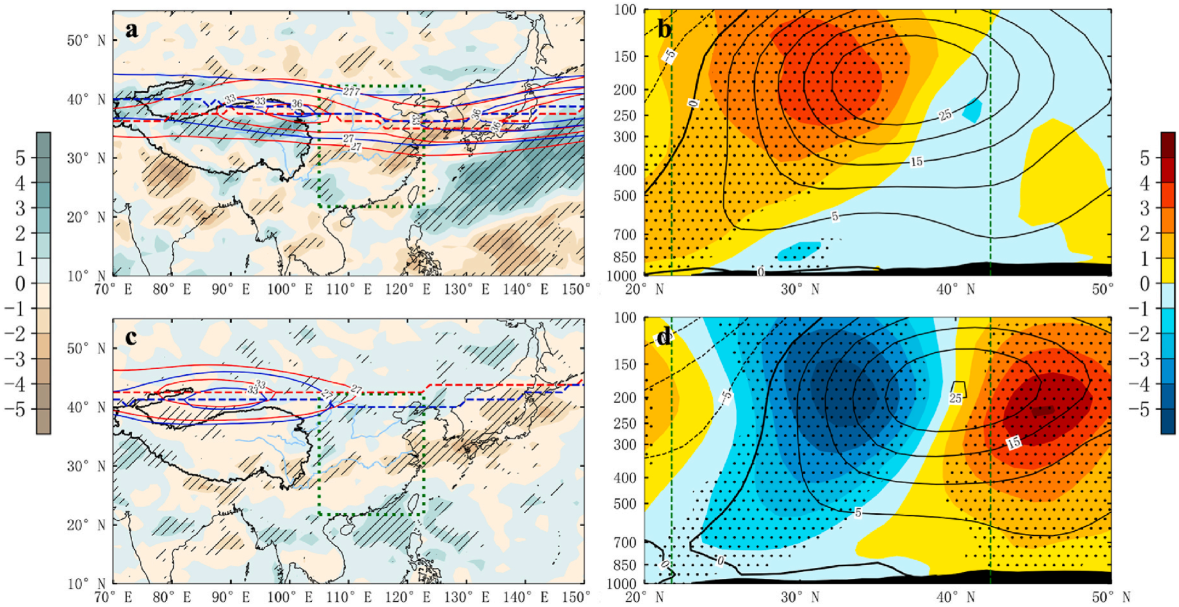

Fig. 5. Spatial configurations of the upper-level atmospheric circulation associated with contrasting TP AHS states during 1981–2020. Panels (a) and (c) show the composite differences of 200 hPa horizontal divergence (shaded, 10^{-6} s^{-1}) in (a) June and (c) JA, respectively; solid red (blue) contours represent the anomalous zonal wind speeds, and dashed lines indicate the core axis of the westerly jet stream under strong (weak) TP AHS conditions. Panels (b) and (d) illustrate the meridional-vertical cross-sections of the differences in zonal wind (shaded, m s^{-1}), with contours indicating the climatological zonal wind (m s^{-1}) for June and JA, respectively. Hatched and dotted regions denote areas exceeding the 90% confidence level. The green boxes delineate the target region of eastern China.

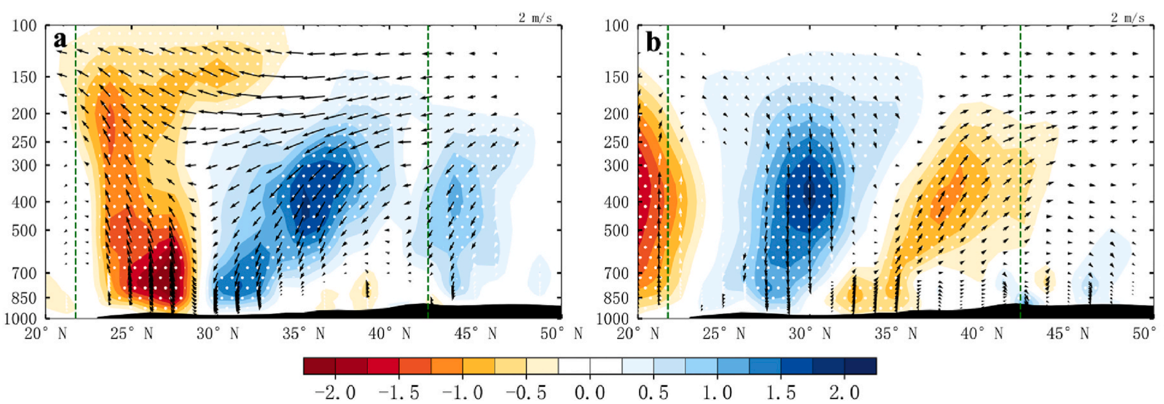

Fig. 6. Meridional-vertical cross-sections of the differences in vertical velocity (shaded, 10^{-2} Pa s^{-1}) and meridional-vertical wind vectors (where vertical velocity is multiplied by 100, and the vector scale is defined by the horizontal component in m s^{-1}) averaged over the eastern China longitudinal band (105°-122.75°E) associated with contrasting TP AHS states during 1981–2020. Panels (a) and (b) show the configurations for June and JA, respectively. Black shading denotes the terrain topography. Black vectors and white dots indicate regions exceeding the 90% confidence level.

the lower troposphere. In accordance with the adiabatic omega equation, this isentropic downglide dynamically necessitates a deep, widespread layer of suppressed vertical motion ($\omega > 0$) and adiabatic compression over the downstream YRV. Conversely, on the western upstream flank, the anomalous easterlies interact with the corresponding temperature gradient in an opposite geometric alignment, promoting complementary isentropic upglide that drives the ascending branch. This intuitive dynamic closure provides a comprehensive explanation for the three-dimensional asymmetric overturning surrounding the TP.

The South Asian High (SAH) and WPSH, two key atmospheric systems modulating East Asian summer climate, demonstrate distinct, month-dependent configuration shifts rather than a uniform seasonal evolution pattern. In June, an enhanced TP AHS is tightly coupled with the concurrent abnormal strengthening and mutual approach of both the upper-level SAH and lower-level WPSH, which characteristically converge south of 30°N (Fig. 8a). Horizontally, the displaced WPSH configuration closely aligns with a well-defined mid-to-lower-level anomalous cyclonic circulation centered over the Korean Peninsula and adjacent waters. Along the western and northwestern peripheries of this anomalous cyclone, robust northerly-to-northeasterly wind anomalies extend directly into the target NCP region (Fig. 8a). Crucially, as substantiated by the 850 hPa thermodynamic diagnostics in Fig. 9a, these significant northerly wind components blow across the regional thermal gradient, establishing a substantial center of positive horizontal temperature advection over the NCP. This specific "northerly-driven warm advection" is fundamentally shaped by early-summer land-sea thermal contrast. During June, the rapidly insolated East Asian landmass becomes significantly warmer than adjacent, relatively cool marine regions. As the anomalous cyclonic circulation scoops this pre-warmed continental air mass from inland and drives it southward via its western peripheral northerlies, it manifests as a distinct back-flow warming mechanism directly over the NCP. Consequently, this low-level horizontal warm advection acts as an additive pathway spatially superimposed onto the upper-level forced adiabatic warming (Figs. 5 and 6).

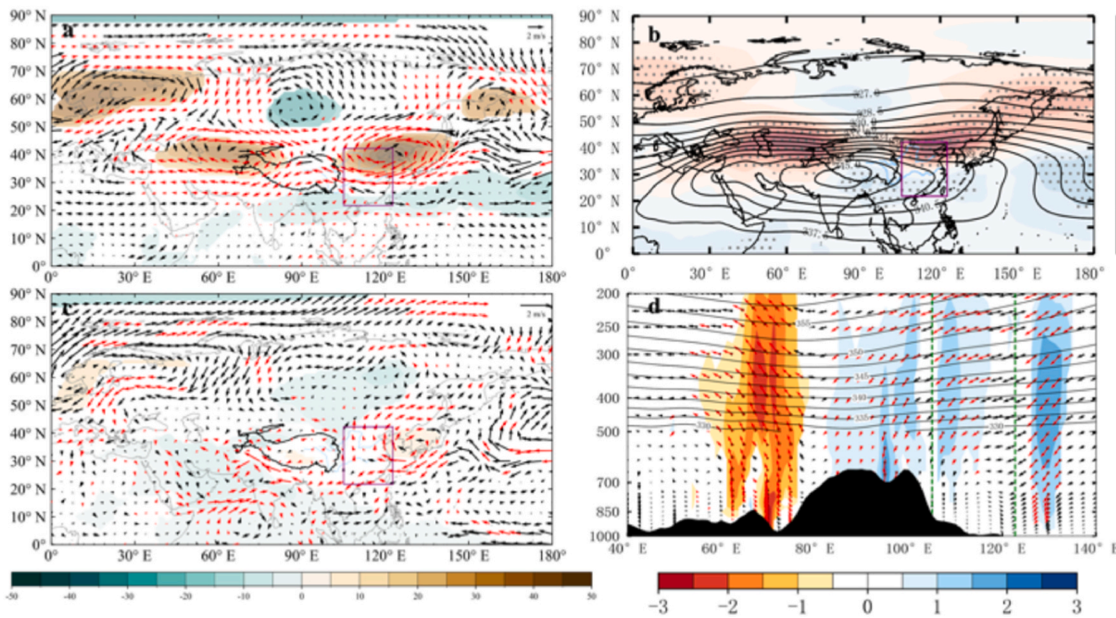

Fig. 7. Anomalous large-scale circulation and thermodynamic structures during JA associated with constrasting TP AHS states from 1981 to 2020. Panels show the composite differences of (a) geopotential height (shaded, gpm) and horizontal wind vectors (m s^{-1}) at 200 hPa, (b) potential temperature (shaded, K) at 200 hPa, (c) geopotential height (shaded, gpm) and horizontal wind vectors (m s^{-1}) at 850 hPa, and (d) zonal-vertical cross section of vertical velocity (shaded, 10^{-2} Pa s^{-1}) and zonal-vertical wind vectors (where vertical velocity is multiplied by 100, and the vector scale is defined by the horizontal component in m s^{-1}) averaged along the target latitudinal band (21.75°-42.25°N). Contours in (b) and (d) indicate the corresponding climatological potential temperature (K) in JA. Red vectors and dotted areas indicate regions denote areas exceeding the 90% confidence level. The domain of eastern China is outlined by purple boxes in (a-c) and green dashed lines in (d).

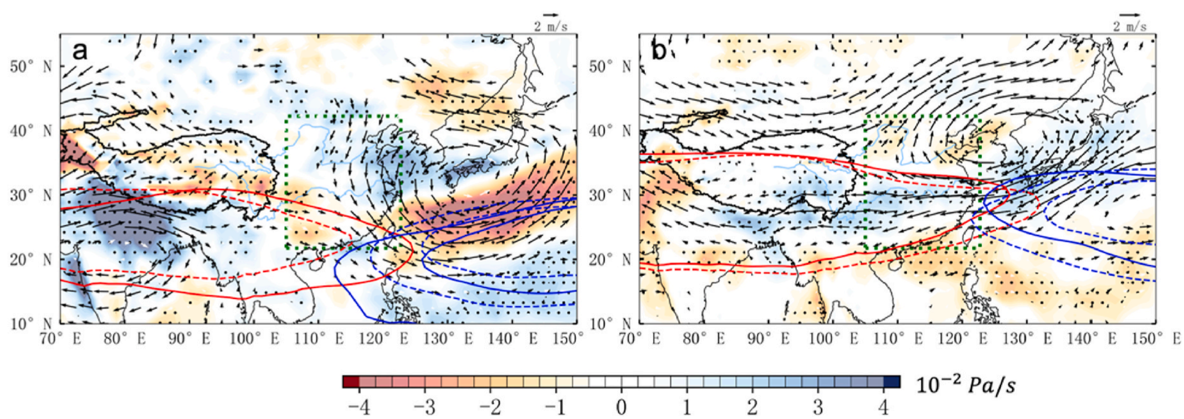

Fig. 8. Composite differences of vertical velocity (shaded, 10^{-2} Pa s^{-1}) and horizontal winds (vectors, m s^{-1}) at 500 hPa in (a) June and (b) JA between strong and weak TP AHS years. Solid and dashed lines represent the 12,500 gpm (red) and 5880/5870 gpm (blue) contours for strong and weak TP AHS years, respectively. Black vectors and dotted areas indicate regions exceeding the 90% confidence level.

These two processes operate at different layers of the atmospheric column, jointly amplifying the sub-seasonal clustering of extreme heatwave events over the NCP.

During peak summer (JA, Fig. 8b), a distinct configuration emerges as both the SAH and WPSH migrate markedly northward, with the SAH extending directly over the YRV region. Under enhanced TP AHS conditions, these two dominant pressure systems exhibit divergent longitudinal movements accompanied by relatively weaker intensities (Fig. 8b). As the WPSH retreats eastward and jumps northward, its northern flank corresponds to a broad low-level easterly wind anomaly, which aligns with the anomalous anticyclone situated further north over the Korean Peninsula (Fig. 8b). However, in stark contrast to the June configuration, these robust lower-level easterly anomalies do not produce positive warm advection over the YRV; instead, they correspond to widespread negative temperature advection (cooling anomalies) across central-eastern China (Fig. 9b). This thermodynamic distribution is inherently constrained by the lower surface temperature of the marine air source relative to the intensely heated landmass during JA. Consequently, the suppressed vertical motion over the YRV during JA is not driven by low-level thermal advection, but is rather dynamically anchored by upper-level ageostrophic processes. Specifically, the northwestward relocation of the SAH leads to pronounced upper-level anomalous convergence aloft (Fig. 5c), which, in tandem with mid-tropospheric isentropic downglide, reinforces the deep subsidence over the YRV.

3.4. Diabatic heating processes

Beyond the atmospheric dynamic processes detailed above, localized thermodynamic and diabatic heating anomalies closely co-vary with the

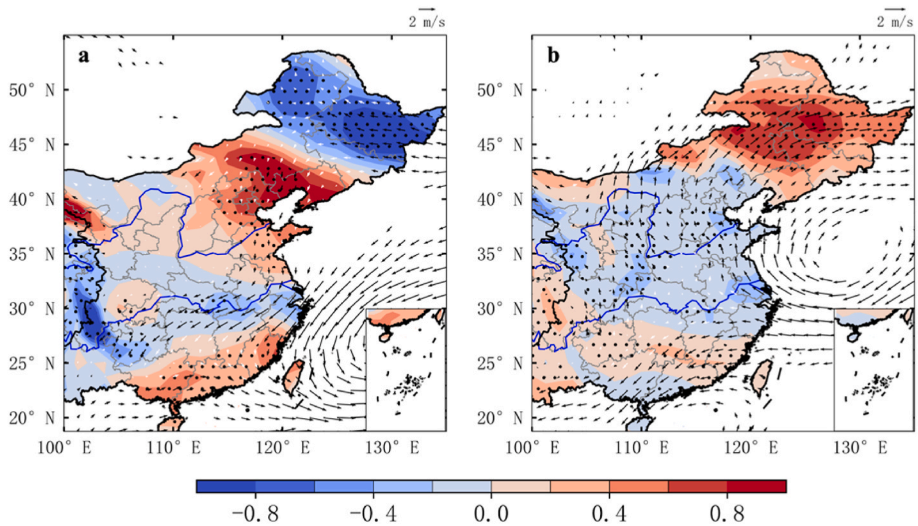

Fig. 9. Composite differences of the horizontal temperature advection (shaded, 10^{-5} K s^{-1}) and wind field (vectors, m s^{-1}) at 850 hPa in (a) June and (b) JA between strong and weak TP AHS years. Dotted areas indicate regions exceeding the 90% confidence level.

sub-seasonal distribution of eastern China heatwaves. Figs. 10 and 11 illustrate the spatial configurations of total cloud cover, surface downward solar radiation flux, and surface sensible heat flux during strong and weak TP AHS years.

During June, a prominent and statistically significant negative total cloud cover anomaly center is localized directly over the NCP (Fig. 10a). This widespread reduction in cloud shields diminishes the regional cloud-albedo reflection, thereby facilitating an enhanced downward shortwave radiation flux reaching the surface, with anomalies exceeding 10 W m^{-2} over the core NCP sector (Fig. 11a). Thermodynamically, this substantial radiative surplus exhibits a strong spatial coupling with the underlying continental surface energy partition, manifesting as a profound intensification of the surface sensible heat flux with positive anomalies exceeding 5 W m^{-2} (Fig. 11c). This enhanced sensible heating configuration structurally co-modulates a favorable thermodynamic background for the localized clustering of June heatwave events over the NCP.

During JA, a distinctly different spatial configuration emerges as the core anomalies shift southward, aligning with the YRV sector. A massive, highly significant negative cloud cover anomaly locks over the YRV, with local decreases approaching −9% (Fig. 10b). Under this clear-sky configuration, the downstream YRV region experiences maximized solar insolation, as evidenced by an extensive patch of significant positive downward solar radiation anomalies exceeding 10 W m^{-2} (Fig. 11b). This intense downward radiative input is spatially synchronized with the escalation of surface sensible heat fluxes over the middle-to-lower reaches of the YRV (Fig. 11d). Consequently, these prominent diabatic configurations, superimposed on the dynamic adiabatic warming aloft, provide a coherent, data-driven depiction of the thermodynamic environments that sustain localized extreme heatwaves across the changing sub-seasonal stages.

4. Summary and discussion

4.1. Summary

In recent years, eastern China has experienced a growing frequency of extreme high-temperature events, resulting in extensive socio-

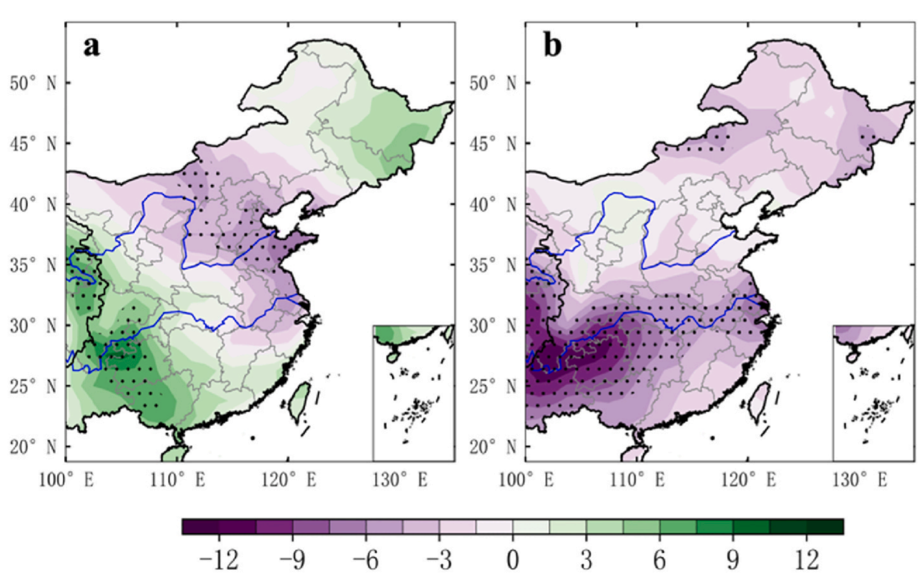

Fig. 10. Composite differences of the total cloud cover (shaded, %) in (a) June and (b) JA between strong and weak TP AHS years. Dotted areas indicate regions exceeding the 90% confidence level.

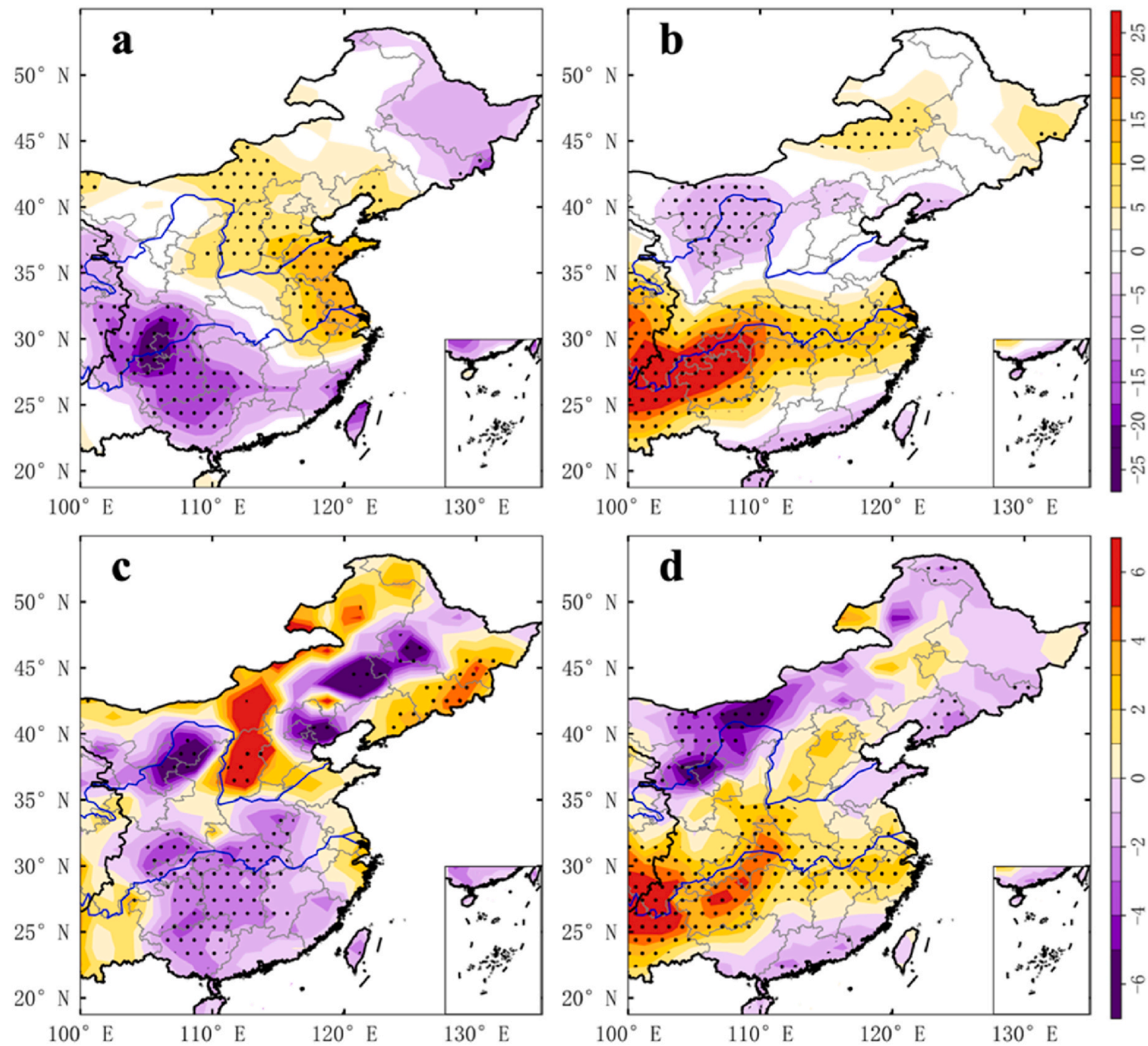

Fig. 11. Composite differences of (a, b) surface downward solar radiation flux and (c, d) surface sensible heat flux (W m^{-2}) in (a, c) June and (b, d) JA between strong and weak TP AHS years. Dotted areas indicate regions exceeding the 90% confidence level.

economic vulnerabilities and significant public health concerns. While previous investigations have identified various atmospheric circulation anomalies linked to East Asian summer heatwaves, they have primarily focused on seasonal-mean conditions or individual case studies. Consequently, the S2S variability and the underlying mechanism transition of extreme heatwaves remain inadequately understood. Targeting this critical timescale, the present study demonstrates that the spatiotemporal heterogeneity of extreme heatwaves across different summer months is closely linked to distinct circulation systems and thermodynamic configurations associated with the TP AHS. The principal findings are summarized as follows.

(1) Extreme heatwaves over eastern China exhibit pronounced S2S variability, characterized by distinct spatial shifts across different summer months. In June, extreme heatwaves predominantly cluster over the NCP, whereas during peak summer (JA), the YRV becomes the primary hotspot. This geographical migration perfectly matches the sub-seasonal evolution of the TP AHS, which exhibits a strong interannual co-variability with these regional warming footprints, accounting for approximately 35% of heatwave occurrences over the NCP in June and 51% over the YRV in JA.

(2) During early summer (June), an intensified TP AHS structurally co-varies with a southward displacement of the upper-level westerly jet stream, enhancing vertical wind shear and producing upper-level differential thermal advection that corresponds to the deep subsidence over the NCP. In the lower troposphere, the strengthened and westward-extended WPSH remains securely positioned south of 30°N. This expansion dynamically shapes an anomalous cyclonic circulation centered over the Korean Peninsula and the adjacent Sea of Japan along the northern flank of the WPSH. Along the western periphery of this cyclonic anomaly, robust northerly-to-northeasterly winds scoop pre-warmed continental air from the intensely insolated East Asian inland. This process drives a substantial back-flow warm advection over the NCP, which, spatially superimposed on the aloft dynamic subsidence warming, jointly accounts for the sub-seasonal clustering of June heatwave events over the NCP.

(3) During peak summer (JA), the enhanced TP AHS is accompanied by a distinctly different dynamic configuration, characterized by a marked northward shift of the westerly jet stream and a northwestward displacement of a weakened SAH. This structural reorganization aligns with the deep subsidence over the YRV. Physically, the northward-displaced jet axis features robust easterly anomalies along its southern flank, which, in tandem

with the characteristic V-shaped isentropic downglide radiating from the TP, presents a coherent tropospheric downwelling over the YRV. Concurrently, the northwestward shift of the SAH places the YRV under a region of anomalous upper-level convergence, establishing a vertically synchronized, deep tropospheric subsidence structure that co-varies with the localized clustering of YRV heatwaves.

(4) Additionally, these dynamic configurations are tightly coupled with coherent localized diabatic-radiative feedback mechanisms that exhibit clear sub-seasonal shifting centers (locking over the NCP in June and the YRV in JA). A significant depletion of total cloud cover matches reduced cloud-albedo reflection, accompanying an enhanced surface downward shortwave radiation flux and a substantial radiative surplus at the surface. This energy input is strongly coupled with the continental surface energy partition, manifesting as a profound intensification of surface sensible heat flux over the planetary boundary layer. This self-reinforcing land-atmosphere thermodynamic loop structurally aligns with the intensity and persistence of localized extreme heatwaves across the changing seasons.

4.2. Discussion

The structural coupling between TP thermal anomalies and downstream extreme heatwaves over eastern China highlights a multi-scale, month-dependent thermodynamic configuration. This study demonstrates that the sub-seasonal variations of TP AHS show a clear spatial alignment with the structural adjustments of the atmospheric circulation and vertical thermodynamic profiles over downstream regions, thereby exhibiting a substantial relationship with the occurrence and development of extreme heatwave events.

Crucially, this sub-seasonal transition highlights a sophisticated seasonal-lock mechanism associated with the abrupt shift of the East Asian westerly jet. Specifically, our diagnostics reveal an intriguing structural asymmetry over the YRV: while this region is subject to upper-level convergence anomalies closely linked with the jet stream configurations in both June and JA (Fig. 5a and c), it exhibits drastically different vertical velocity responses. In June, despite the presence of localized upper-level convergent forcing aloft, the YRV remains tightly embedded within the strong climatological westerly jet core and is heavily accompanied by the robust northward-advancing monsoon moisture and strong convective diabatic heating, which effectively counteracts the large-scale dynamic downwelling signal. In contrast, during JA, the massive poleward retreat of the jet stream core allows the jet-exit ageostrophic convergence to phase-lock and synergistically couple with the anomalous upper-level easterly flow. Consequently, the forced dynamic subsidence smoothly extends downward without convective obstruction, establishing deep adiabatic compression that matches the clustering of localized extreme heatwaves over the YRV.

Additionally, this state-dependence emphasizes that the downstream impact of TP AHS is non-isolated; rather, it co-varies in concert with broader planetary-scale drivers and interannual climate modes. To address the potential confounding influences of external ocean–atmosphere boundary forcings, partial correlation analyses were conducted by removing the concurrent signals of the El Niño–Southern Oscillation (ENSO) and the Indian Ocean Dipole (IOD). Notably, even after partialling out these dominant climate modes, the significant statistical association between the TP AHS and downstream extreme heatwaves persists robustly over the key target regions during both June and JA (Fig. S8 and 9). This critical piece of evidence strongly implies that the TP AHS possesses a relatively independent and intrinsic dynamical link with eastern China heatwaves, rather than acting as a mere passive reflection of major tropical oceanic variances. Nevertheless, it should be acknowledged that our current partial correlation framework primarily controls for tropical oceanic drivers (ENSO and IOD). Preceding land surface boundary conditions—most notably spring TP snow cover—can serve as a plausible common forcing that modulates both the summer TP thermal anomalies and downstream East Asian circulation (Wu et al., 2012, 2016). Accounting for such lagged land-atmosphere coupling effects remains a residual limitation of the present diagnostic scheme and warrants further quantitative disentanglement in future work.

However, in alignment with the intrinsic complexity of the climate system, this independent relationship does not preclude the existence of bidirectional thermodynamic feedbacks or concurrent external modulations. Both the TP AHS and downstream circulation anomalies remain embedded within a larger web of mid-to-high-latitude atmospheric variability (e.g., circumglobal wave trains, polar vortex shifts) and local land–atmosphere feedbacks (e.g., soil moisture and vegetation conditions) (Zhang et al., 2021; Tan et al., 2023). Therefore, while the statistical link is highly robust and clear of major tropical artifacts, the observed simultaneous alignment should be interpreted as a synergistic, mutually amplifying co-variation under specific seasonal-lock backgrounds, rather than an unassailable, one-way linear causal trajectory.

Furthermore, to ensure the physical robustness of these diagnostic relationships and verify that the identified sub-seasonal thermodynamic configurations are not statistical artifacts of our specific composite baseline, a rigorous threshold sensitivity test was conducted. The strong and weak TP AHS years were re-selected using a stricter criterion based on the 90th and 10th percentile thresholds of the timeseries. Crucially, under this extreme percentile framework, the key dynamical signatures—including the upper-level jet-exit ageostrophic convergence, deep tropospheric subsidence over the YRV, and multi-scale circulation anomalies—remain qualitatively identical and highly robust, with the spatial patterns changing very little compared to our original composites (figures not shown). This robust consistency demonstrates that the synoptic-scale co-variations described herein represent highly stable, intrinsic features of the East Asian climate system rather than being sensitive to arbitrary threshold choices.

Despite growing attention to the physical mechanisms of extreme heatwaves, many key questions remain unresolved. First, the relative fractional contributions of different drivers—including TP thermal features—are still poorly quantified, particularly in terms of their spatial and temporal heterogeneity across eastern China. Second, the potential nonlinear interactions between multi-scale systems remain largely unexplored. In particular, the possible synergistic amplification between TP thermal anomalies and large-scale circulation patterns (such as the subtropical high and westerly jet) warrants deeper investigation. To address these gaps, future research should prioritize three aspects: (1) integrating multi-source observational and reanalysis datasets to enhance spatiotemporal resolution; (2) employing high-resolution numerical models to capture fine-scale land–atmosphere and circulation interactions; and (3) combining dynamical and statistical attribution frameworks (e.g., intraseasonal phase-composite diagnostics and high-resolution numerical sensitivity experiments) to disentangle and precisely determine the temporal precedence, phase-leading ISO dynamics, and fractional contributions of different forcing mechanisms under varying climate regimes. Such efforts will be instrumental in advancing our scientific understanding of compound drivers of extreme heat and will also support the development of more accurate forecasts and early warning systems for heatwaves under a changing climate.

CRediT authorship contribution statement

Meirong Wang: Writing – review & editing, Writing – original draft, Methodology, Conceptualization. **Shuaiyi Li:** Software, Formal analysis. **Zhongshui Yu:** Visualization, Validation. **Zhu Zhu:** Visualization, Validation. **Jun Wang:** Writing – review & editing.

Declaration of competing interest

The authors declare the following financial interests/personal relationships which may be considered as potential competing interests:

Jun Wang reports financial support was provided by National Natural Science Foundation of China. If there are other authors, they declare that they have no known competing financial interests or personal relationships that could have appeared to influence the work reported in this paper.

Acknowledgments

This work was jointly funded by the National Natural Science Foundation of China (Grant 42475129), and Xizang science and technology plan project (XZ202602YD0006).

Appendix A. Supplementary data

Supplementary data to this article can be found online at https://doi.org/10.1016/j.wace.2026.100955.

Data availability

The JRA-55 reanalysis data can be freely accessed on the website https://rda.ucar.edu/ dssearch/?words = Jra55. The daily precipitation CN05.1 can be freely accessed on the website https://ccrc.iap.ac.cn/resource.

References

Alizadeh, M.R., Abatzoglou, J.T., Adamowski, J.F., Prestemon, J.P., Chittoori, B., Asanjan, A.A., Sadegh, M., 2022. Increasing heat-stress inequality in a warming climate. Earths Future 10, 1–11.

Arblaster, J.M., Alexander, L.V., 2012. The impact of the El Niño–Southern Oscillation on maximum temperature extremes. Geophys. Res. Lett. 39, L20702.

Bretherton, C.S., Widmann, M., Dymnikov, V.P., Wallace, J.M., Bladé, I., 1999. The effective number of spatial degrees of freedom of a time-varying field. J. Clim. 12, 1990–2009.

Cao, D.R., Xu, K., Huang, Q.L., Tam, C.Y., Chen, S., He, Z.Q., Wang, W.Q., 2022. Exceptionally prolonged extreme heat waves over south China in early summer 2020: the role of warming in the tropical Indian ocean. Atmos. Res. 278, 106335.

Chen, G.X., Iwasaki, T., Qin, H.L., Sha, W.M., 2014. Evaluation of the warm-season diurnal variability over East Asia in recent Reanalyses JRA-55, ERA-Interim, NCEP CFSR, and NASA MERRA. J. Clim. 27, 5517–5537.

Chen, X., Zhou, T., 2018. Relative contributions of external SST forcing and internal atmospheric variability to July–August heat waves over the Yangtze River valley during 1979–2014. Clim. Dyn. 51, 4403–4419.

Choi, W., Kim, K.Y., 2019. Summertime variability of the western North Pacific subtropical high and its synoptic influences on the East Asian weather. Sci. Rep. 9, 7865.

Deng, K., Yang, S., Gu, D., Lin, A., Li, C., 2020. Record-breaking heat wave in southern China and delayed onset of South China Sea summer monsoon driven by the Pacific subtropical high. Clim. Dyn. 54, 3751–3764.

Deng, K., Yang, S., Ting, M.F., Zhao, P., Wang, Z.Y., 2019. Dominant modes of China summer heat waves driven by global Sea surface temperature and atmospheric internal variability. J. Clim. 32 (12), 3761–3775.

Deng, Z., Zhou, S., Wang, M., Cai, Y., Ma, Y., Yang, C., Sun, Y., 2023. Changes in the midsummer extreme high-temperature events over the Yangtze River valley associated with the thermal effect of the Tibetan Plateau and Arctic Oscillation. Atmos. Res. 293, 106911.

Diallo, I., Xue, Y., Chen, Q., Ren, X., Guo, W., 2022. Effects of spring Tibetan Plateau land temperature anomalies on early summer floods/droughts over the monsoon regions of South East Asia. Clim. Dyn. 62, 2659–2681.

Dong, L., Xu, X., Zhao, T., Ren, H., 2019. Linkage between moisture transport over the Yangtze River Basin and a critical area of the Tibetan Plateau during the Meiyu. Clim. Dyn. 53, 2643–2662.

Dong, W., Jia, X., Li, X., Wu, R., 2024b. Synergistic effects of Arctic amplification and Tibetan Plateau amplification on the Yangtze River Basin heatwaves. npj Clim. Atmos. Sci. 7, 150.

Dong, W., Jia, X., Wu, R., 2024a. Intensified impact of spring Tibetan Plateau snow cover on summer compound heat waves in western Europe after 1998. J. Clim. 37 (8), 2423–2441.

Duan, A., Wu, G., Zhang, Q., Liu, Y., 2006. New proofs of the recent climate warming over the Tibetan Plateau as a result of the increasing greenhouse gases emissions. Chin. Sci. Bull. 51, 1396–1400.

Freychet, N., Tett, S., Wang, J., Hegerl, G., 2017. Summer heat waves over eastern China: dynamical processes and trend attribution. Environ. Res. Lett. 12, 024015.

Ge, J., You, Q.L., Zhang, Y.Q., 2019. Effect of Tibetan Plateau heating on summer extreme precipitation in eastern China. Atmos. Res. 218, 364–371.

Hao, Z.C., Chen, Y., Feng, S.F., Liao, Z., An, N., Li, P.X., 2023. The 2022 Sichuan-Chongqing spatio-temporally compound extremes: a bitter taste of novel hazards. Sci. Bull. 68 (13), 1337–1339.

He, C., Zhou, J.J., Zhang, L.X., Chen, X.L., Zhang, W.X., 2023. Extremely hot east Asia and flooding western south Asia in the summer of 2022 tied to reversed flow over Tibetan Plateau. Clim. Dyn. 61, 2103–2119.

He, W., Chen, H., 2024. Anthropogenic influence has increased the nighttime heat stress risks in eastern China. Earths Future 12, e2023EF004406.

Hu, S., Zhou, T., Peng, D., Jiang, W., Lu, B., Wu, B., Chen, X., Zhang, L., Zhang, W., 2024. Extreme dry advection dominates the record-breaking Yangtze River heatwave in midsummer of 2022. Clim. Dyn. 62, 5049–5060.

IPCC, 2021. Climate Change 2021: the Physical Science Basis. Contribution of Working Group I to the Sixth Assessment Report of the Intergovernmental Panel on Climate Change. Cambridge University Press.

Jiang, J.L., Liu, Y.M., Mao, J.Y., Wu, G.X., 2023. Extreme heatwave over Eastern China in summer 2022: the role of three oceans and local soil moisture feedback. Environ. Res. Lett. 18 (4), 044025.

Jiang, J.L., Liu, Y.M., Meng, J., Wu, G.X., He, B., Ma, T.T., Bao, W., Fan, J.F., 2024. Dry soil moisture on the Tibetan plateau drives synchronous extreme heatwaves in Europe and East Asia. npj Clim. Atmos. Sci. 7, 281.

Jiang, W., Ding, T., Gao, H., Lv, Z., 2024. China's Yangtze River basin is becoming the super heatwave centre in the east Asian monsoon regions. Int. J. Climatol. 44 (14), 5028–5038.

Jiang, Y., Li, Z., Zeng, G., Zhou, B., Shao, Y., 2025. Interannual relationship between the extreme high temperature frequency over the Yangtze River basin and the North Atlantic sea surface temperature anomaly in summer. Clim. Dyn. 63, 125.

Kang, S.C., Eltahir, E.A.B., 2018. North China Plain threatened by deadly heatwaves due to climate change and irrigation. Nat. Commun. 9, 2894.

Kobayashi, S., Yukinari, O., Yayoi, H., Ayataka, E., Masami, M., Hirokatsu, O., Kazutoshi, O., Hirotaka, K., Chiaki, K., Hirokazu, E., Kengo, M., Kiyotoshi, T., 2015. The JRA-55 reanalysis: general specifications and basic characteristics. J. Meteorol. Soc. Jpn. Ser. II 93, 5–48.

Kong, D.D., Xie, Y.X., Gu, X.H., Slater, L., Ci, H., Song, H.Y., 2024. Contribution of anthropogenic activities to the intensification of heat index-based spatiotemporally contiguous heatwave events in China. J. Geophys. Res. Atmos. 129 (3), e2023JD040004.

Li, J., Ding, T., Jia, X., Zhao, X., 2015. Analysis on the extreme heat wave over China around Yangtze River region in the summer of 2013 and its main contributing factors. Adv. Meteorol., 706713

Li, N., Xiao, Z.N., Zhao, L., 2021. A recent increase in long-lived heatwaves in China under the joint influence of south Asia and western north Pacific subtropical highs. J. Clim. 34 (17), 7167–7179.

Li, X., Hu, Z., Liu, Y., Liang, P., Jha, B., 2023. Causes and predictions of 2022 extremely hot summer in east Asia. J. Geophys. Res. Atmos. 128 (13), e2022JD038442.

Liang, P., Zhang, Z., Ding, Y., Hu, Z., Chen, Q., 2024. The 2022 extreme heatwave in Shanghai, lower reaches of the Yangtze River Valley: combined influences of multiscale variabilities. Adv. Atmos. Sci. 41, 593–607.

Liang, W., Li, C., Wu, Y., Zou, M., Zhu, X., Dong, W., Moore, J., Liu, F., Qiao, S., Dong, T., Wang, K., Chen, D., 2024. Anthropogenic forcing and subtropical anticyclonic drivers of the August 2022 heatwave in China. Weather Clim. Extrem. 45, 100707.

Lin, X., Wang, Y., Song, L., 2024. Urbanization amplified compound hot extremes over the three major urban agglomerations in China. Geophys. Res. Lett. 51, e2023GL106644.

Liu, Q., Zhou, T.J., Mao, H.T., Fu, C.B., 2019. Decadal variations in the relationship between the western pacific subtropical high and summer heat waves in eastern China. J. Clim. 32, 1627–1640.

Lu, G.M., Li, Q.Q., Sun, X.T., Zhao, M.C., Dong, L.L., Wu, Q.Y., Wang, L.J., Zhao, L., Duan, C.F., Yin, Y.Z., Wang, P.L., Shen, X.Y., 2024. Comparative analysis of peak-summer heatwaves in the Yangtze–Huaihe River Basin of China in 2022 and 2013: thermal effects of the Tibetan Plateau. Atmos. Res. 300, 107222.

Luo, M., Lau, N.C., 2018. Amplifying effect of ENSO on heat waves in China. Clim. Dyn. 52, 3277–3289.

Luo, Y.Y., Wang, S., Zhang, L., Tian, B., Jia, J.J., Sun, W.J., et al., 2025. Comparative evaluation of reanalysis-derived temperature profile and low-level temperature inversion on the Tibetan Plateau. Res. Cold Arid Regions. https://doi.org/10.1016/j.rcar.2025.08.004.

Ma, K.J., Gong, H.N., Wang, L., Fang, H.J., Chen, W., 2025. Comparison of extreme heatwaves in southern China in August 2022 and 2024. Atmos. Res. 321, 108116.

Ma, S., Zhou, T., Stone, D.A., Angélil, O., Shiogama, H., 2017. Attribution of the July–August 2013 heat event in central and eastern China to anthropogenic greenhouse gas emissions. Environ. Res. Lett. 12, 054020.

Ni, Y.Y., Qiu, B., Miao, X., Li, L.F., Chen, J.Y., Tian, X.H., Zhao, S.W., Guo, W.D., 2024. Shift of soil moisture-temperature coupling exacerbated 2022 compound hot-dry event in eastern China. Environ. Res. Lett. 19, 014059.

Peng, J., Yuan, X., Ma, F., Xu, Q., 2024. Drivers of long-term changes in summer compound hot extremes in China: climate change, urbanization, and vegetation greening. Atmos. Res. 310, 107632.

Peng, Y., Wang, Q., Zhai, P., 2024. Differentiated influences of anomalous subtropical high on extreme persistent precipitation and heatwave events in the Yangtze River valley. Q. J. Roy. Meteorol. Soc. 150 (765), 4856–4869.

Piao, S., Ciais, P., Huang, Y., Shen, Z.H., Peng, S.S., Li, J.S., Zhou, L.P., Liu, H.Y., Ma, Y. C., Ding, Y.H., Friedlingstein, P., Liu, C.Z., Tan, K., Yu, Y.Q., Zhang, T.Y., Fang, J.Y., 2010. The impacts of climate change on water resources and agriculture in China. Nature 467, 43–51.

Qian, C., Ye, Y.B., Jiang, J.C., Zhong, Y.Y., Zhang, Y.T., Pinto, I., Huang, C.R., Li, S.H., Wei, K., 2023. Rapid attribution of the record-breaking heatwave event in North China in June 2023 and future risks. Enciron. Res. Lett 19, 014028.

Qian, Z.H., Sun, Y.X., Ma, Q.R., Gu, Y., Feng, T.C., Feng, G.L., 2024. Understanding changes in heat waves, droughts, and compound events in Yangtze River valley and the corresponding atmospheric circulation patterns. Clim. Dyn. 62, 539–553.
Robine, J.M., Cheung, S.L.K., Le Roy, S., Oyen, H.V., Griffiths, C., Michel, J.P., Herrmann, F.R., 2008. Death toll exceeded 70,000 in Europe during the summer of 2003. C. R. Biol. 331, 171–178.
Shi, J.Q., Yao, Y., Guo, R.W., Luo, B.H., Zhong, L.H., 2025. The intensifying relationship between heatwaves in the mid-lower reaches of the Yangtze River valley and the upstream atmospheric wave train after the 2000s. Atmos. Res. 313, 107770.
Shi, P., Leung, L.R., Lu, H., Wang, B., Yang, K., Chen, H.S., 2024. Uncovering the interannual predictability of the 2003 European summer heatwave linked to the Tibetan Plateau. npj Clim. Atmos. Sci. 7, 242.
Sun, X., Ren, G., Ren, Y., 2022. Observed changes in extreme temperature over China during 1961–2018. J. Meteorol. Res. 36 (1), 1–15.
Sun, Y., Hu, T., Zhang, X., 2018. Substantial increase in heat wave risks in China in a future warmer world. Earths Future 6, 1528–1538.
Sun, Y., Zhang, X., Zwiers, F., Song, L., Wan, H., Hu, T., Ying, H., Ren, G., 2014. Rapid increase in the risk of extreme summer heat in eastern China. Nat. Clim. Change 4, 1082–1085.
Tan, J., Wang, J., Wang, H., Liu, Z., Zeng, N., Yan, R., et al., 2024. Influence of extreme 2022 heatwave on megacities' anthropogenic CO_2 emissions in lower-middle reaches of the Yangtze River. Sci. Total Environ., 175605
Tan, Z., Liu, Y., Shao, T., Luo, R., Luo, M., Xie, Y., 2023. Association between Tibetan heat sources and heat waves in China. J. Clim. 36, 7905–7924.
Tan, Z., Liu, Y., Tang, W., Li, D., Gao, J., Luo, M., 2025. Impact of the tibetan plateau heat source on heatwaves in China. Clim. Dyn. 63, 2.
Tao, P.H., Zhang, Y.C., 2019. Large-scale circulation features associated with the heat wave over Northeast China in summer 2018. Atmos. Ocean. Sci. Lett. 12 (4), 254–260.
Wang, J., Yan, R., Wu, G., Liu, Y., Wang, M., Zeng, N., et al., 2023. Unprecedented decline in photosynthesis caused by summer 2022 record-breaking compound drought-heatwave over Yangtze River Basin. Sci. Bull. 68, 2160–2163.
Wang, M., Guo, D., Zhong, S., 2019a. Comparision of the multi-source datasets in calculation of the atmospheric heat sources over the Tibetan Plateau. Meteo.Mon 45 (12), 1718–1726 (in Chinese).
Wang, M., Wang, J., Duan, A., Yang, J., Liu, Y., 2019b. Quasi-biweekly impact of the atmospheric heat source over the Tibetan Plateau on summer rainfall in eastern China. Clim. Dyn. 53, 4489–4504.
Wang, W., Zhou, W., Li, X., Wang, X., Wang, D., 2016. Synoptic- scale characteristics and atmospheric controls of summer heat waves in China. Clim. Dyn. 46, 2923–2941.
Wang, Z., Luo, H., Yang, S., 2023. Different mechanisms for the extremely hot central-eastern China in July–August 2022 from a Eurasian large-scale circulation perspective. Environ. Res. Lett. 18.
Wu, G., Duan, A., Liu, Y., Mao, J., Ren, R., Bao, Q., He, B., Liu, B., Hu, W., 2015. Tibetan Plateau climate dynamics: recent research progress and outlook. Natl. Sci. Rev. 2, 100–116.
Wu, G., Liu, Y., Zhang, Q., Duan, A., Wang, T., Wan, R., Liu, X., Li, W., Wang, Z., Liang, X., 2007. The influence of mechanical and thermal forcing by the Tibetan Plateau on Asian climate. J. Hydrol. 8, 770–789.
Wu, J., Gao, X.J., 2013. A gridded daily observation dataset over China region and comparison with the other datasets. Chin. J. Geophys. 56, 1102–1111 (in Chinese).
Wu, Z., Jiang, Z., Li, J., Zhong, S., Wang, L., 2012. Possible association of the western Tibetan Plateau snow cover with the decadal to interdecadal variations of northern China heatwave frequency. Clim. Dyn. 39, 2393–2402.
Wu, Z., Zhang, P., Chen, H., Li, Y., 2016. Can the Tibetan Plateau snow cover influence the interannual variations of Eurasian heat wave frequency? Clim. Dyn. 46, 3405–3417.
Xiao, H.W., Xu, P.Q., Wang, L., 2024. The unprecedented 2023 North China heatwaves and their S2S predictability. Geophys. Res. Lett. 51 (6), e2023GL107642.
Yanai, M., Esbensen, S., Chu, J.H., 1973. Determination of bulk properties of tropical cloud clusters from large-scale heat and moisture budget. J. Atmos. Sci. 30, 611–627, 1973.
Yang, X.C., Chen, F., Zhu, W.P., Teng, W.P., 2015. Urbanization effects on observed changes in summer extreme heat events over Zhejiang Province, east China. J. Trop. Meteorol. 21 (3), 295–302.
Yao, T., Xue, Y., Chen, D., 2019. Recent third pole's rapid warming accompanies cryospheric melt and water cycle intensification and interactions between monsoon and environment. B AM Meteorol. Soc. 100 (3), 423–444.
Zhai, P.M., Pan, X.H., 2003. Trends in temperature extremes during 1951–1999 in China. Geophys. Res. Lett. 30 (17), 1913.
Zhang, M.M., Dong, B.W., Schiemann, R., Robson, Jon, 2024. Summer compound heatwaves over China: projected changes at different global warming levels and related physical processes. Clim. Dyn. 62, 1887–1907.
Zhang, Y., Mao, G., Chen, C., Shen, L., Xiao, B., 2021. Population exposure to compound droughts and heatwaves in the observations and ERA5 reanalysis data in the Gan River Basin, China. Land 10, 1021.
Zhang, Y., Sun, Y., Hu, T., 2024. Changes in extreme high temperature warning indicators over China under different global warming levels. Sci. China Earth Sci. 67, 1895–1909.
Zhao, W., 2020. Extreme weather and climate events in China under changing climate. Natl. Sci. Rev. 7, 938–943.
Zheng, Z., Lin, X., Chen, L., Yan, C., Sun, T., 2024. Effects of urbanization and topography on thermal comfort during a heat wave event: a case study of Fuzhou, China. Sustain. Cities Soc. 102, 105233.
Zhou, X.Y., Li, Y., Xiao, C., Chen, W., Mei, M., Wang, G.F., 2025. High-impact extreme weather and climate events in China: summer 2024 overview. Adv. Atmos. Sci. https://doi.org/10.1007/s00376-024-4462-6.
Zhu, Z., Wang, M., Wang, J., Duan, A., Liu, B., Yu, Z., 2025. Intraseasonal oscillation intensity variations of the atmospheric heat source over the Tibetan Plateau and their relationship with summer precipitation. J. Clim. 38 (4), 931–946.